Wide-Field Imaging of Superconductor Vortices with Electron Spins in Diamond

Yechezkel Schlussel,[1,*] Till Lenz,[2,3,*] Dominik Rohner,[4] Yaniv Bar-Haim,[1] Lykourgos Bougas,[2] David Groswasser,[1] Michael Kieschnick,[5] Evgeny Rozenberg,[1] Lucas Thiel,[4] Amir Waxman,[1] Jan Meijer,[5] Patrick Maletinsky,[4] Dmitry Budker,[2,3,6] and Ron Folman[1,†]

[1] *Department of Physics, Ben-Gurion University of the Negev, Be'er Sheva 84105, Israel*

[2] *Johannes Gutenberg-Universität Mainz, 55128 Mainz, Germany*

[3] *Helmholtz Institut Mainz, 55099 Mainz, Germany*

[4] *Department of Physics, University of Basel, Basel CH-4056, Switzerland*

[5] *Faculty of Physics and Earth Sciences, Felix Bloch Institute for Solid State Physics, Leipzig University, 04103 Leipzig, Germany*

[6] *Department of Physics,University of California, Berkeley, California 94720-7300, USA*

(Received 6 April 2018; revised manuscript received 25 June 2018; published 18 September 2018)

Understanding the mechanisms behind high-T_c type-II superconductors (SCs) is still an open task in condensed-matter physics. One way to gain further insight into the microscopic mechanisms leading to superconductivity is to study the magnetic properties of the SCs in detail, for example, by studying the properties of vortices and their dynamics. In this work, we describe a method of wide-field imaging magnetometry using nitrogen-vacancy (NV) centers in diamond to image vortices in an yttrium-barium-copper-oxide (YBCO) thin film. We demonstrate quantitative determination of the magnetic-field strength of the vortex stray field, the observation of vortex patterns for different cooling fields, and direct observation of vortex pinning in our disordered YBCO film. This method opens prospects for imaging of the magnetic-stray fields of vortices at frequencies from dc to several megahertz within a wide range of temperatures, which allows for the study of both high-T_C and low-T_C SCs. The wide temperature range allowed by NV center magnetometry also makes our approach applicable for the study of phenomena like island superconductivity at elevated temperatures (e.g., in metal nanoclusters).

DOI: 10.1103/PhysRevApplied.10.034032

I. INTRODUCTION

Studying the physics of vortices in type-II superconductors (SCs) is a key challenge in the field of condensed-matter physics, which, in the past, has been addressed by various methods. For example, a scanning superconducting quantum-interference device (SQUID) [1–4], scanning Hall-probe magnetometry [5–7], Bitter decoration [8–10], transmission-electron microscopy (TEM)[11,12], scanning tunneling microscopy and spectroscopy [13], Lorentz microscopy [14], and magneto-optical imaging [15,16] have been used to image vortices in type-II superconductors. Recently, a method has been proposed [17] and realized [18], which uses a single nitrogen-vacancy (NV) center in a scanning diamond tip to study such vortices. Using NV centers enables quantitative noninvasive studies of the vortices over a wide temperature range, which is not achievable with the previously mentioned methods. In this work, ensembles of NV centers in diamond are used for an alternative approach of imaging vortices. Utilizing ensembles has the important advantage of not requiring a physical scan of the sample (or the sensor), thereby opening the door for fast imaging up to video frame rates [19]. Here, we use this technique in a wide-field microscope to image vortices in an yttrium-barium-copper-oxide (YBCO) thin film.

NV centers in diamond are point defects in the diamond lattice and have a magnetic-field-dependent energy-level splitting, which can be driven by resonant microwaves and read out optically by excitation with green light and collection of red NV fluorescence [20]. Magnetometry with NV centers is a widely used technique because of its combination of sensitivity and high spatial resolution. It is applicable in a wide temperature range from cryogenic to ambient temperatures [18,21,22]; in addition, the method enables the determination of both the absolute value and the direction of the magnetic field [20,23,24].

II. EXPERIMENTAL SETUP

The experimental setup located at Ben-Gurion University of the Negev incorporates a wide-field-imaging

*These authors contributed equally to this work

†folman@bgu.ac.il

microscope [see Fig. 1(a)] with the imaging target placed in a continuous-flow helium cryostat. The superconducting sample, a thin YBCO film (thickness ≈ 250 nm), is placed onto the cold finger inside the cryostat and a diamond microslab (thickness ≈ 2 μm) with {100} surfaces is placed flat on top of the superconductor. The proper engineering of the SC-diamond interface and, in particular, the resulting NV-SC distance is a crucial enabling factor for this work. Commonly used diamond plates of dimensions on the order of $3 \times 3 \times 0.5$ mm^3 do not allow us to detect individual vortices. Because of the distance between the diamond plate and the SC, it is only possible to measure the averaged homogeneous field penetrating the SC [25]. In addition, the properties of the NV centers in the used diamond plates are not able to detect a magnetic field below 0.1 mT [see Sec. III and Fig. 1(c)]. This result means that, in order to observe individual vortices, the distance between the SC and diamond has to be below approximately 1 μm. To achieve this, thin diamond plates with dimensions of $20 \times 10 \times 2$ μm^3, with a near-surface NV-center rich layer of approximately 70-nm thickness, are fabricated and placed onto the SC (see Appendix). Microwave fields are applied by a wire [see Fig. 1(a), inset], which is mounted on the homebuilt cryostat window to keep the heat transfer to the SC as low as possible, while still keeping the wire close to the diamond. The fluorescence is detected using a CCD camera with a pixel size of 16×16 μm^2.

III. RESULTS

A. Optically detected magnetic-resonance images

To generate vortices, the sample is field-cooled in a magnetic field of approximately 0.18 mT, applied perpendicular to the surface of the YBCO film. Optically detected magnetic-resonance (ODMR) spectra are taken for every pixel of the camera, each of which corresponds to an area of 0.16×0.16 μm^2 on the sample. The ODMR spectra are obtained by comparing NV fluorescence rates with and without applied microwaves while scanning the MW frequency from 2.84 to 2.91 GHz. The fluorescence contrast is calculated as $C = (N_{\mathrm{on}} - N_{\mathrm{off}})/(N_{\mathrm{on}} + N_{\mathrm{off}})$, where $N_{\mathrm{on(off)}}$ is the photon detection rate, while the applied microwave field is on (off). The NV-center ground state is a spin-1 system, leading to three states with $m_s = -1$, 0, and $+1$. In the absence of symmetry-breaking fields, the $m_s = \pm 1$ states are degenerate, leading to the same transition frequency from the $m_s = 0$ state to the $m_s = \pm 1$ states of 2.87 GHz at room temperature (2.88 GHz at cryogenic temperatures). The transition frequencies get split by a magnetic field along the NV axis where the splitting is given by $\Delta\nu_{\pm 1} = 2\gamma_{\mathrm{NV}} B_{\mathrm{NV}}$, with $\gamma_{\mathrm{NV}} = 28$ MHz/mT and B_{NV} the magnetic field along the NV axis. For our diamond samples and at temperatures slightly above the SC phase transition, even at zero field, a splitting (approximately 6 MHz) in the ODMR spectra occurs due to strain in the diamond lattice [20]. This strain mixes the $m_s = \pm 1$ states, so that m_s are no longer good quantum numbers, and results in

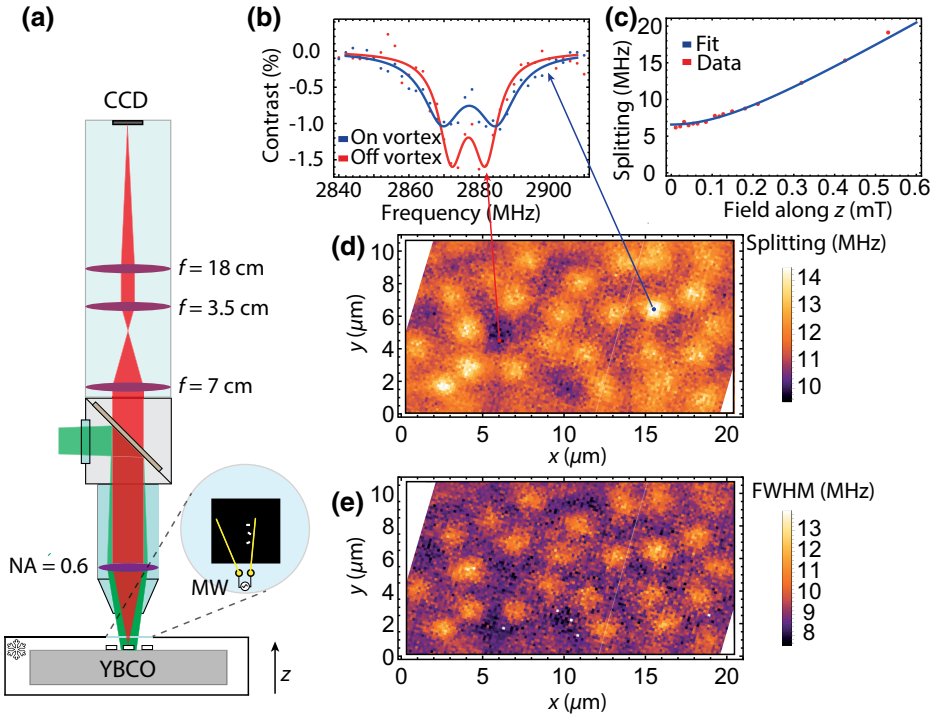

FIG. 1. (a) Schematic of the experimental setup. (b) ODMR spectrum for a pixel on top of the vortex and for a pixel outside of the vortex stray field, which is approximately 0.38 mT in the center of the vortex. (c) Calibration of the magnetic field in the nonlinear regime at low fields. (d) Map of the splitting between the two ODMR peaks. (e) Map of the width of the ODMR peaks. Vortices are identified by an increase in the splitting between the ODMR peaks, which is attributed to the magnetic stray field of the vortices. In addition, the vortices' stray field leads to a broadening of the peaks, which is generated by field inhomogeneities over the detection volume. The acquisition time for the images (d),(e) is approximately 11 min.

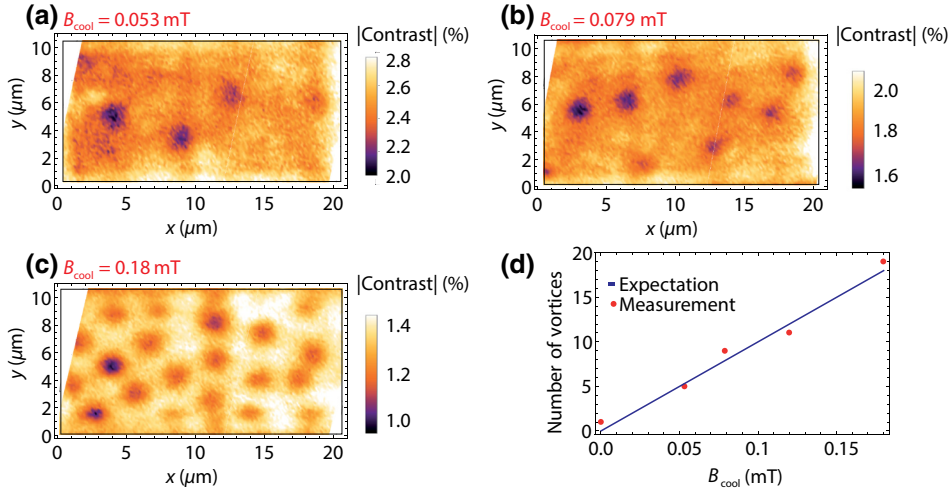

FIG. 2. (a)–(c) Single-frequency images (acquisition time of approximately 80 s) of vortices obtained using microwaves resonant with the NV-spin transition at zero magnetic field (2.876 GHz). Images are taken for a magnetic field (B_{cool}) present during the cooling through the metal-superconductor phase transition with $B_{\mathrm{cool}} = 0.053$, 0.079, and 0.18 mT. An increase in the number of vortices can be observed when the field is increased. (d) The observed number of vortices as well as the expected number of vortices in the given field of view of 200 μm^2 for different fields.

a nonlinear relation of $\Delta\nu_{\pm1}(B_{\mathrm{NV}}) = 2\sqrt{(\gamma_{\mathrm{NV}}B_{\mathrm{NV}})^2 + E^2}$, with E being the strain splitting for low magnetic fields [26]. For ensembles of NV centers, there are in general four different NV axes with corresponding different field projections that need to be considered. For the {100} diamonds used in this work, the field projection for a field perpendicular to the surface is the same for all NV orientations.

To determine the ODMR splitting, the recorded data are fitted to two Lorentzians [Fig. 1(b)] for each pixel, and color maps of the peak width and splitting between the peaks are created [Figs. 1(d) and 1(e)]. The splitting of the two peaks differs by approximately 4 MHz depending on the point of observation with respect to the vortex center. Additionally, the width of the peaks also changes by an amount of 4 MHz, which is attributed to magnetic-field gradients averaged over the optical resolution of approximately 500 nm and to vibrations that are of similar magnitude as the optical resolution. To illustrate these effects more explicitly, Fig. 1(b) shows two ODMR spectra, one recorded on a vortex and one far from a vortex. Even though the change in splitting is on the same order as the splitting due to strain at zero field (see below), it is possible to determine the magnetic field above the vortices. To do this, we calibrate the splitting between the two peaks as a function of magnetic field by applying a known, out-of-plane magnetic field to the diamond and the data are fitted [see Fig. 1(c)] using the relation mentioned above. The angle between the NV centers and the applied field is considered by using $B_{\mathrm{NV}} = B_z/\sqrt{3}$ and the strain splitting E is determined to be 3.29 (5) MHz.

Using this calibration, we determine the maximum field perpendicular to the SC above the vortices to be between approximately 0.36 and 0.4 mT. Following the model used in Ref. [27] and considering a bulk London penetration depth $\lambda_L = 250$ nm [18], we see that these fields correspond to an average distance between the YBCO and the NV layer of approximately 550 nm. This distance is larger than expected from the roughnesses of the SC (approximately 100 nm) and the diamond plate (approximately 3 nm) and the depth of the diamond layer ($d_{\mathrm{NV}} \approx 15$–$85$ nm) and it probably originates from dust particles on the surface of the SC and outliers in the roughness of the SC. Decreasing the distance between the SC and the diamond in the future would shrink the observed size of the vortices and allow us to extract more precise information on the magnetic field.

B. Single-frequency images

To reduce the image acquisition time, instead of taking whole ODMR spectra for every pixel, images of vortices are obtained by determining the contrast for every pixel for only a single MW frequency (e.g., 2.876 GHz) applied to drive the NV spins. The magnetic field of the vortex leads to a splitting of this resonance and, therefore, to an increased fluorescence at the position of the vortices in

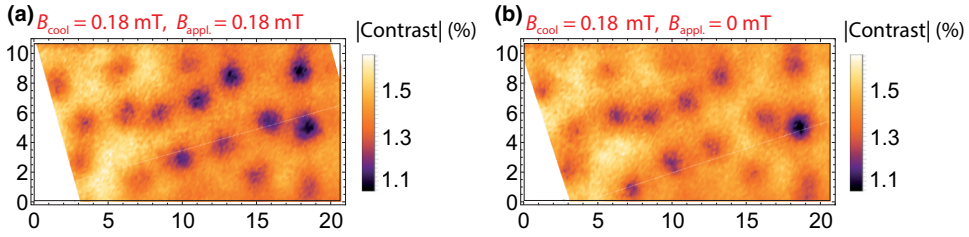

FIG. 3. (a) A single-frequency map (acquisition time of approximately 80 s) with the applied magnetic field. (b) A map after the magnetic field is turned off after reaching the SC phase. Both pictures show the same vortex pattern due to strong pinning in the SC sample.

the presence of the MW-driving field (see Fig. 2). These images are taken for different cooling fields, ranging from $B_{\mathrm{cool}} \approx 0$ to 0.18 mT, applied along the direction normal to the SC film. As expected, the different cooling fields led to different vortex densities in the SC. The expected number of vortices is $N = B_{\mathrm{cool}}A/\Phi_0$, where $\Phi_0 = h/(2e) = 2.07$ mT μm^2 is the magnetic flux quantum, B_{cool} is the magnetic field during cooldown to the SC phase, and A is the investigated area. For the dimensions of our sensitive area, which is the area of the diamond microslab of 200 μm^2, this leads to $N/B \approx 100$ mT^{-1}. Figure 2(d) compares the measured number of vortices with the theoretical expectation and shows good agreement between the two.

C. Pinning

Another important phenomenon in type-II SC is pinning [28], where the magnetic flux (i.e., vortices) is trapped within the SC due to disorder, even when the external field is turned off. This effect is associated with defects in the superconductor that pin the vortices into their positions. To study pinning, a single-frequency image of the vortex distribution, with and without the applied magnetic field after the cooldown, are taken (Fig. 3). The same vortices can be identified in both images, which means that the pinning is strong enough to trap all the vortices that were previously created, extending the results of an earlier study using ensembles of NV centers [25], where individual vortices could not be resolved.

IV. CONCLUSION

A technique is presented enabling wide-field imaging of vortices in SCs using NV centers in diamond. By using microfabricated diamond plates, it is possible to reduce the sample-NV distance, which allows us to study the stray magnetic field of vortices in a type-II SC. ODMR spectra are obtained to determine the magnetic-field magnitude from which the distance between the SC and diamond is calculated to be less than 1 μm. It is possible to reduce the acquisition time for an entire image using a single frequency. Single-frequency images are taken for different cooling fields and the obtained number of vortices is compared to the theoretical expectations. In addition, pinning of the vortices in the SC is observed. To improve this technique, one could, for example, use a diamond with less strain to enhance the sensitivity at low magnetic fields or use a {111} diamond with preferential NV-center orientation [29], leading to an increase in contrast. In addition, the use of a diamond with {111} surfaces would align the NV axis of one of the orientations with the magnetic field of the vortices and, therefore, increase the resulting splitting in the ODMR spectrum. Future experiments will focus on more detailed studies of the vortices and their dynamics, such as vortex oscillations in their pinning potential. Using the presented method, such oscillations can be sensed from dc up to several MHz [22,30]. The implementation of pulsed measurement schemes would in addition enhance the sensitivity to ac fields [20,31]. Moreover, this technique can be applied as a universal tool to precisely measure the magnetic structures of thin films and/or surfaces.

ACKNOWLEDGMENTS

We thank Louis Bouchard, Andrey Jarmola, Victor M. Acosta, and Vladimir Z. Kresin for fruitful discussions. This work is supported in part by the DFG DIP Grant No. FO 703/2-1, by Swiss NFS Grants No. 142497 and No. 155845, and by the Swiss Nanoscience Institute. This work is also partially supported by the Israeli Science Foundation.

APPENDIX A: SAMPLE PREPARATION

The diamond plates are fabricated using electron-beam lithograpy lithography and plasma etching [32] of an "optical grade" Element 6 diamond (produced via chemical vapor deposition (CVD)) with {100} surfaces and an initial nitrogen concentration below 1 ppm. The NV-rich layer close to the surface of the diamond is created using ion implantation of nitrogen ions with energies of 10, 35, and 50 keV. The diamond is subsequently annealed at 800°C for 10 h and at 1200°C for 2 h to form the NV centers. Assuming a conversion efficiency of approximately 5% [33], this process results in a NV-center density of approximately 3.7 ppm within the implanted layer. This result corresponds to a mean separation of approximately 11.4 nm between the NV centers. The plates are broken out of an array [34] using a micromanipulator and then placed on the SC. In this procedure, we cannot control whether the implanted side is facing toward the diamond. To increase the probability of finding a diamond positioned with the correct orientation, several plates are placed on top of the SC. For a superconductor, a commercially available YBCO thin film from Ceraco consisting of 250 nm of YBCO grown on a sapphire wafer with a 40-nm buffer of CeO_2 is used. This configuration leads to an orientation of the YBCO c axis perpendicular to the surface of the thin film. The critical temperature of the SC sample is approximately 87 K (according to the company specifications). In addition, we are able to transfer the diamond plates to other samples using a sharp needle. This is due to the fact that electrostatic forces between the needle and the diamond are stronger than the van der Waals forces between the SC and the diamond. The low van der Waals interaction is consistent with the surface roughness and the unexpectedly large distance between the SC and diamond plate.

APPENDIX B: EXPERIMENTAL SETUP

The experimental setup consists of a continuous-flow helium cryostat (Janis model ST-500) and a homebuilt wide-field fluorescence microscope. The green excitation light is generated by a Gem 532 laser (Laser Quantum) reflected with a dichroic mirror (Semrock FF635-Di01-25x36) and focused onto the sample with an Olympus LUCPLFLN40XRC objective with a $\times 40$ magnification and a NA $= 0.6$. The fluorescence is collected through the same path; after it traverses the dichroic mirror and a telescope (to increase the magnification by a factor of 2), it is focused on the camera [Andor iXon 897 electron-multiplying charge-coupled device (EMCCD) camera, with pixel size $16 \times 16\ \mu m^2$] with a 180-mm tube lens.

[1] L. Emban, Y. Anahory, A. Suhov, D. Halbertal, J. Cuppens, A. Yakovenko, A. Uri, Y. Myasoedov, M. L. Rappaport, M. E. Huber, A. Gurevich, and E. Zeldov, Probing dynamics and pinning of single vortices in superconductors at nanometer scales, Sci. Rep. **5**, 7598 (2015).

[2] B. Kalisky, J. R. Kirtley, J. G. Analytis, J.-H. Chu, A. Vailionis, I. R. Fisher, and K. A. Moler, Stripes of increased diamagnetic susceptibility in underdoped superconducting $Ba(Fe_{1-x}Co_x)_2As_2$ single crystals: Evidence for an enhanced superfluid density at twin boundaries, Phys. Rev. B **81**, 184513 (2010).

[3] L. Embon, Y. Anahory, Ž. L. Jelić, E. O. Lachman, Y. Myasoedov, M. E. Huber, G. Mikitik, A. V. Silhanek, M. V. Milošević, A. Gurevich, and E. Zeldov, Imaging of super-fast dynamics and flow instabilities of superconducting vortices, Nat. Commun. **8**, 85 (2017).

[4] A. Kremen, S. Wissberg, N. Haham, E. Persky, Y. Frenkel, and B. Kalisky, Mechanical control of individual superconducting vortices, Nano Lett. **16**, 1626 (2016).

[5] B. Raes, J. V. de Vondel, A. V. Silhanek, C. C. de Souza Silva, J. Gutierrez, R. B. G. Kramer, and V. V. Moshchalkov, Local mapping of dissipative vortex motion, Phys. Rev. B **86**, 064522 (2012).

[6] D. Cole, S. Bending, S. Sael'ev, A. Grigorenko, T. Tamegai, and F. Nori, Ratchet without spatial asymmetry for controlling the motion of magnetic flux quanta using time-asymmetric drives, Nat. Mater. **5**, 305 (2006).

[7] A. M. Chang, H. D. Hallen, H. F. Hess, H. L. Kao, J. Kwo, A. Sudbø, and T. Y. Chang, Scanning hall-probe microscopy of a vortex and field fluctuations in $L_{1.85}Sr_{0.15}CuO_0$ films, Europhys. Lett. **20**, 645 (1992).

[8] I. V. Grigorieva, Magnetic flux decoration of type-II superconductors, Supercond. Sci. Technol. **7**, 161 (1994).

[9] S. Rablen, M. Kemmler, T. Quaglio, R. Kleiner, D. Koelle, and I. V. Grigorieva, Bitter decoration of vortex patterns in superconducting Nb films with random, triangular, and Penrose arrays of antidots, Phys. Rev. B **84**, 184520 (2011).

[10] Y. Fasano, M. D. Seta, M. Menghini, H. Pastoriza, and F. de la Cruz, Commensurability and stability in nonperiodic systems, Proc. Natl. Acad. Sci. USA **102**, 3898 (2005).

[11] J. A. Xia, N. J. Long, N. Strickland, P. Hoefakker, E. F. Talantsev, X. Li, W. Zhang, T. Kodenkandath, Y. Huang, and M. W. Rupich, TEM observation of the microstructure of metal-organic deposited $YBa_2Cu_3O_{x-\delta}$ with Dy additions, Supercond. Sci. Technol. **20**, 8 (2007).

[12] J. C. Loudon, S. Yazdi, T. Kasama, N. D. Zhigadlo, and J. Karpinski, Measurement of the penetration depth and coherence length of MgB_2 in all directions using transmission electron microscopy, Phys. Rev. B **91**, 054505 (2015).

[13] O. Fischer, M. Kugler, I. Maggio-Aprile, C. Berthod, and C. Renner, Scanning tunneling spectroscopy of high-temperature superconductors, Rev. Mod. Phys. **79**, 353 (2007).

[14] K. Harada, Lorentz microscopy observation of vortices in high-t_c superconductors using a 1 mv field emission transmission microscope, Microscopy **62**, S3 (2013).

[15] P. E. Goa, H. Hauglin, M. Baziljevich, E. Il'yachenko, P. L. Gammel, and T. H. Johansen, Real-time magneto-optical imaging of vortices in superconducting $NbSe_2$, Supercond. Sci. Technol. **14**, 729 (2001).

[16] S. J. Bending, Local magnetic probes of superconductors, Adv. Phys. **48**, 449 (1999).

[17] L.-S. Bouchard, V. M. Acosta, E. Bauch, and D. Budker, Detection of the Meissner effect with a diamond magnetometer, New J. Phys. **13**, 025017 (2011).

[18] L. Thiel, D. Rohner, M. Ganzhorn, P. Appel, E. Neu, B. Müller, R. Kleiner, D. Koelle, and P. Maletinsky, Quantitative nanoscale vortex imaging using a cryogenic quantum magnetometer, Nat. Nanotechnol. **11**, 677 (2016).

[19] A. Horsley, P. Appel, J. Wolters, J. Achard, A. Tallaire, P. Maletinsky, and P. Treutlein, Microwave device characterisation using a widefield diamond microscope, [quant-ph].

[20] L. Rondin, J.-P. Tetienne, T. Hingant, J.-F. Roch, P. Maletinsky, and V. Jacques, Magnetometry with nitrogen-vacancy defects in diamond, Rep. Prog. Phys. **77**, 056503 (2014).

[21] V. M. Acosta, E. Bauch, M. P. Ledbetter, A. Waxman, L.-S. Bouchard, and D. Budker, Temperature Dependence of the Nitrogen-Vacancy Magnetic Resonance in Diamond, Phys. Rev. Lett. **104**, 070801 (2010).

[22] V. M. Acosta, E. Bauch, A. Jarmola, L. J. Zipp, M. P. Ledbetter, and D. Budker, Broadband magnetometry by infrared-absorption detection of nitrogen-vacancy ensembles in diamond, Appl. Phys. Lett. **97**, 174104 (2010).

[23] K. Jensen, P. Kehayias, and D. Budker, *High Sensitivity Magnetometers*. Springer International Publishing, 2017, p. 553.

[24] G. Chatzidrosos, A. Wickenbrock, L. Bougas, N. Leefer, T. Wu, K. Jensen, Y. Dumeige, and D. Budker, Miniature Cavity-Enhanced Diamond Magnetometer, Phys. Rev. Appl. **8**, 044019 (2017).

[25] A. Waxman, Y. Schlussel, D. Groswasser, V. M. Acosta, L.-S. Bouchard, D. Budker, and R. Folman, Diamond magnetometry of superconducting thin films, Phys. Rev. B **89**, 54509 (2014).

[26] M. W. Doherty, F. Dolde, H. Fedder, F. Jelezko, J. Wrachtrup, N. B. Manson, and L. C. L. Hollenberg, Theory of the ground-state spin of the NV^- center in diamond, Phys. Rev. B **85**, 205203 (2012).

[27] G. Carneiro and E. H. Brandt, Vortex lines in films: Fields and interactions, Phys. Rev. B **61**, 6370 (2000).

[28] G. Blatter, M. V. Feigel'man, V. B.Geshkenbein, A. I. Larkin, and V. M. Vinokur, Vortices in high-temperature superconductors, Rev. Mod. Phys. **66**, 1125 (1994).

[29] M. Lesik, J.-P. Tetienne, A. Tallaire, J. Achard, V. Mille, A. Gicquel, J.-F. Roch, and V. Jacques, Perfect preferential orientation of nitrogen-vacancy defects in a synthetic diamond sample, Appl. Phys. Lett. **104**, 113107 (2014).

[30] C. S. Shin, C. E. Avalor, M. C. Butler, D. R. Trease, S. J. Seltzer, J. P. Mustonen, D. J. Kennedy, V. M. Acosta, D. Budker, A. Pines, and V. S. Bajaj, Room temperature operation of a radiofrequency diamond magnetometer near the shot noise limit, J. Appl. Phys. **112**, 124519 (2012).

[31] N. Aslam, M. Pfender, P. Neumann, R. Reuter, A. Zappe, F. F. de Oliveira, A. Denisenko, H. Sumiya, S. Onoda, J. Isoya, and J. Wrachtrup, Nanoscale nuclear magnetic resonance with chemical resolution, Science **357**, 67 (2017).

[32] P. Appel, E. Neu, M. Ganzhorn, A. Barfuss, M. Batzer, M. Gratz, A. Tschöpe, and P. Maletinsky, Fabrication of all diamond scanning probes for nanoscale magnetometry, Rev. Sci. Instrum. **87**, 063703 (2016).

[33] S. Pezzagna, B. Naydenoc, F. Jelezko, J. Wrachtrup, and J. Meijer, Creation efficiency of nitrogen-vacancy centres in diamond, New J. Phys. **12**, 065017 (2010).

[34] D. Riedel, D. Rohner, M. Ganzhorn, T. Kaldewey, P. Appel, E. Neu, R. J. Warburton, and P. Maletinsky, Low-Loss Broadband Antenna for Efficient Photon Collection from a Coherent Spin in Diamond, Phys. Rev. Appl. **2**, 064011 (2014).